Statistical computation of thermal conductivity in neutron star matter "pastas"

Guillermo A. Frank* Claudio O. Dorso† Alejandro Strachan‡

Abstract

This investigation explores the energy transportation occurring in nuclear star matter, as it undergoes the "topological" transition to the "pasta" regime. We measured the nucleonic thermal conductivity by sampling the energy of nucleons along a well-established heat flux. Our results show that a dramatic change in the conductivity accompanies the "pasta" breakdown. A decoupling phenomenon is also observed for the nucleonic conductivity, depending on the "pasta" topology.

Key Words: Nuclear Star Matter, Thermal Conductivity, Nucleonic Conductivity, Sampling nucleons' energy

1. Introduction

The thermal conductivity across the "inner crust" of a neutron star is expected to be sensitive to temperature and the fraction of species [1, 2]. Although it was first accepted for the protons and neutrons conductivity (κ_p and κ_n, respectively) to be negligible with respect to that of electrons [3], researchers pointed out that κ_p and κ_n can actually influence the thermal relaxation of a neutron star [4, 5, 1, 6, 2].

The effect of nucleon thermal conductivity on the late-time cooling of neutron stars is somewhat controversial throughout the literature. The observed late-time cooling of neutron stars was shown to be consistent with low thermal conductivities [7]. However, the existence of "impurities" in the *pasta* environment had to be postulated in order to match the right cooling curve [2]. Also, the finding of "spiral defects" within this context was considered as an additional source of electron scattering [7, 8].

Regardless of the existence of defects in the *pasta* environment, the true "effective" conductivity remains rather uncertain. Variations of an order of magnitude may be expected due to the alignment of the *pasta* structures with respect to the radial axis of the star [2]. Randomly oriented "*pasta* slabs" may reduce the conductivity by 37%, according to molecular dynamics simulations reported in Ref. [2].

*Unidad de Investigación y Desarrollo de las Ingenierías, Universidad Tecnológica Nacional, Facultad Regional Buenos Aires, Av. Medrano 951, 1179 Buenos Aires, Argentina

†Instituto de Física de Buenos Aires, Pabellón I, Ciudad Universitaria, 1428 Buenos Aires, Argentina.

‡School of Materials Engineering, Purdue University.

Our concern is placed on the "inner" crust situation at low to moderate temperatures. The *pasta* phase is expected to dominate the topological scene at the sub-saturation densities [9, 10]. This topological regime has already been studied in the context of the equation of state (EoS) [11, 10, 9]. But research on the thermal conductivity still focuses on the energy carried by electrons, disregarding the energy flux due to collisions between nuclear species [1, 2, 12]. Other research areas have insisted on the role of the non-electronic heat carriers in lattice-like or liquid-like systems [13, 14].

We will focus on the heat conduction due to nucleons in the *pasta* regime. We presume that topological structures may enhance or hinder the energy transport due to nuclear carriers, as first observed in Ref. [15]. We will consider, however, that nucleons are embedded in an electron gas environment, in order to accomplish a charge-neutral system of nucleons and electrons. The term "thermal conductivity" in this context means the "phononic" or "lattice" contribution to the thermal conductivity. No further mention to the electron contribution will be done.

The investigation is organized as follows. Section 2 summarizes the theoretical background for the thermal conductivity κ in the context of the molecular dynamics model (MD). Section 3 explains the preparations for measuring κ within the *pasta* scenario. The corresponding results are exhibited in Section 4. For clarity reasons, we separated the analysis into symmetric and non-symmetric matter. Our conclusions are presented in Section 5.

2. Background

We use classical molecular dynamics (CMD) to characterize the thermal transport of nuclear star matter. This approach naturally drives the system to its free energy minima within a very complex energy landscape given by the inter-particle interactions and boundary conditions. Literature results on the validity of this approach can be found in Refs. [10, 9, 16, 17, 18].

2.1 The potentials

Nuclear matter is considered as a three particle system composed of protons, neutrons and electrons. The latter, however, is envisaged as a gas that actually introduces a screening effect on the Coulomb potential between protons. The potentials for neutron-proton (np), neutron-neutron (nn) and proton-proton (pp) interactions were first set by Pandharipande to attain a binding energy at the saturation density of $E(\rho_0) = -16\,\mathrm{MeV/nucleon}$ and a compressibility of 250 MeV. The electrons screening effect was later introduced through a Thomas-Fermi potential with an "effective" screening length λ of 20 fm [19]. The whole set reads as follows

Parameter	Value	Units
V_r	3097.0	MeV
V_a	2696.0	MeV
V_0	379.5	MeV
μ_r	1.648	fm^{-1}
μ_a	1.528	fm^{-1}
μ_0	1.628	fm^{-1}
λ	10	fm
r_c	5.4	fm
r_c'	20	fm

Table 1: Parameter set for the CMD computations (New Medium model).

$$
\begin{aligned}
V_{np}(r) &= \frac{V_r}{r}e^{-\mu_r r} - \frac{V_r}{r_c}e^{-\mu_r r_c} - \frac{V_a}{r}e^{-\mu_a r} + \frac{V_a}{r_c}e^{-\mu_a r_c} \\
V_{nn}(r) &= \frac{V_0}{r}e^{-\mu_0 r} - \frac{V_0}{r_c}e^{-\mu_0 r_c} \\
V_{pp}(r) &= V_{nn}(r) + \frac{q^2}{r}e^{-r/\lambda} - \frac{q^2}{r_c'}e^{-r_c'/\lambda}
\end{aligned}
\tag{1}
$$

where q is the electron charge and r_c, r_c' are the cutoff distances for the Pandharipande an Thomas-Fermi potentials, respectively. The value for the parameters appearing in Eq. 1 can be seen in Table 1.

2.2 The thermal conductivity

The thermal conductivity κ corresponds to the set of transport coefficients relating the heat flux (*i.e.* energy flux $\mathbf{J}$) to the temperature gradient ∇T, through the (phenomenological) Fourier law

$$\mathbf{J}(t) = -\kappa\,\nabla T \tag{2}$$

where κ corresponds to a second rank 3×3 tensor for non-isotropic matter. Notice that the constitutive relation (2) is intended as a "macroscopic" one, whenever matter is considered as a continuum. The energy flux $\mathbf{J}$ represents a somewhat "mean" flux density $\langle \mathbf{j} \rangle$ transported across a small volume $\mathcal{V}$ (that is, $\mathbf{J} = \langle \mathbf{j} \rangle . \mathcal{V}$). The calculation of thermal transport properties from atomistic simulations is well established.[20, 21, 22, 23]

We will only consider those situations where $\mathbf{J}$ and ∇T are collinear (say, for example, along the $\hat{z}$ axis) and use a non-equilibrium method for computing the thermal conductivity κ_z is proposed by Müller-Plathe (see Ref. [20]) from the average heat flux and temperature gradient.

$$\kappa_z = -\lim_{t\to\infty} \frac{\langle J_z \rangle}{\langle \partial T/\partial z \rangle} \tag{3}$$

If the medium is isotropic, common practice sets the mean thermal conductivity as $(k_x + k_y + k_z)/3$.

Notice that the linear nature of Eqs. (2) and (3) requires relatively small temperature gradients.

In a nutshell, the Müller-Plathe procedure [20] generates a heat flux of known magnitude and the temperature gradient is obtained as local averages of the kinetic energy. The system is divided in thin bins along the the heat flux direction (see Fig. 1 for details); the first slab is labeled as the "cold" slab, while the slab in the middle is labeled as "hot". A heat flux is generated by exchanging the velocities of two particles (with the same mass), the hottest particle in the "cold" bin and the coldest one in the "hot" bin (see Fig. 1). Thus, the system is (artificially) driven out of equilibrium, and a heat flux **J** develops through the system of interest in the opposite direction for the equilibrium restoration. This flux is expected to reach the stationary state if the exchanging rate is held regularly for a long time.

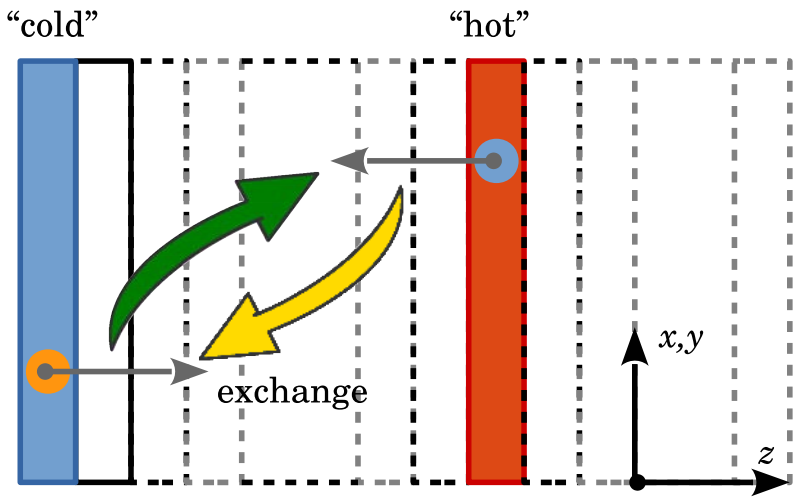

Figure 1: (On-line color only) Schematic representation of the Müller-Plathe procedure. The blue and red bins correspond the the "cold" and "hot" slabs, respectively. The horizontal flat arrows stand for the particles velocity. The curved arrows (green and yellow, respectively) represent the velocity exchange process.

In order to generate an external heat flux, particle velocity exchanges are performed periodically during the MD simulation. Recall that the species themselves are not exchanged, but only the velocities. Thus, the "pumping" process only transports kinetic energy (for particles with the same mass). This procedure conserves total energy and linear momentum.

The heat flux introduced by the velocity exchange is hard to compute from dynamical magnitudes. The computation from the net transported (kinetic) energy is somewhat easier since

$$\langle J_z \rangle + \frac{1}{2A_{xy}} \left[\frac{1}{\tau} \sum_{n=1}^{T} \frac{1}{2} m (v_h^2 - v_c^2) \right] = 0 \tag{4}$$

where the expression between the square brackets represents the mean (kinetic) energy exchanged during the time period τ. v_h and v_c refers to the velocities of the hot particle and cold particle, respectively. The factor $2A_{xy}$ corresponds to the cross section of the slabs (two faces).

The temperature profile is obtained by computing the local (kinetic) temperature for each slab. Once steady state is reached, the temperature profile is expected to be linear away from the cold and hot bins where velocities are exchanged, provided the heat flux remains small. Further details can be found in Ref. [20].

We stress the fact that the balance condition (4) links the heat flux **J** to the (artificial) kinetic energy transportation introduced by the Müller-Plathe procedure. The velocity exchange is not restricted to pairs of similar particles, but also across species (with the same mass). Therefore, the procedure enables the computation of the thermal conductivity for the set of *all* the nucleons, or for the set of protons and neutrons separately. The meaning of either coefficients, though, will be quite different.

3. Simulations

At a first instance, the system was cooled from $T = 4\,\mathrm{MeV}$ down to the solid (pasta) state (say, $T = 0.1\,\mathrm{MeV}$). The density ρ ranged from $0.03\,\mathrm{fm}^{-3}$ to $0.05\,\mathrm{fm}^{-3}$. Nice *lasagnas* or *spaghettis* resulted after the cooling, although not completely aligned to the canonical axes (see below). In order to improve the alignment, we softened the *pasta* by raising the bath temperature to $0.8 - 1.2\,\mathrm{MeV}$, and then, we performed the corresponding transformations. The *pasta* was finally cooled back to $0.1\,\mathrm{MeV}$.

At a second instance, the bath temperature was increases from $0.1\,\mathrm{MeV}$ to $2.1\,\mathrm{MeV}$, while the nucleons' positions and velocities were recorded at regular time intervals. The recorded configurations were set as the initial conditions for the thermal conductivity measurements.

The thermal conductivities reported in Section 4 correspond to those obtained following the Müller-Plathe procedure (see Ref. [20]). Data was collected after a steady state was reached from each initial condition (within the fluctuations typical of small systems). Recall that the Müller-Plathe procedure is known to attain a precision of 10% (on a system of 2600 Lennard-Jones particles [20]).

The Müller-Plathe procedure requires the binning of the primary cell, in order to compute the temperature gradient across the bins (that is, along the heating flux direction). This is why we demanded a proper alignment of the *pasta* with respect to the canonical axes. We set the number of bins to 20.

For each pasta topology we computed two values of the thermal conductivity: "parallel" and "transverse". The former corresponds to the heat flux along the *pasta*. The latter corresponds to the heat flux running across the *pasta*. Each measurement were computed separately.

Whatever the heat flux direction, we computed the thermal conductivity by either flipping the protons' and neutrons' velocity separately, and *all* the nucleons regardless of their nature. The former means that only one specie contributes to the velocity exchange in Eq. (4). This distinction became very useful when analyzing non-symmetric matter (see Section 4.2).

4. Results

4.1 The thermal conductivity κ of symmetric matter

We first computed the thermal conductivity for symmetric neutron star matter ($x = 0.5$) as a function of temperature in the $0.1 - 2.1\,\mathrm{MeV}$ range. This includes the solid-liquid transition ($T \sim 0.5$ MeV) and the topological transition ($T \sim 1\,\mathrm{MeV}$). The computation was carried out in two ways: by considering the heat flux due to *all* the nucleons, or, considering only *one* kind on nucleons (say, the protons; see Section 3 for details). Fig. 2a shows the proton thermal conductivity for a wide temperature range. Fig. 2b shows the details of the smoothed data computations obtained for either protons and *all* the nucleons.

Two regimes can be distinguished immediately according to Fig. 2. The thermal conductivity exhibits a smooth slope above $T \simeq 1.25\,\mathrm{MeV}$, while a dramatic change occurs below this threshold. The later appears as a "decoupling" between the thermal conductivity parallel to the *lasagna* (κ_z) and the one orthogonal to this direction (κ_x). The "decoupling" pattern is essentially the same whether all the nucleons are considered or only the protons (for $x = 0.5$).

It can be noticed in Fig. 2 that the conductivity for *all* the nucleons appears somewhat shifted up with respect to the protons' conductivity. The large fluctuations in the data do not allow a definite conclusion on this phenomenon. However, a small bias seems reasonable due the (local) density of the considered specie (say, nucleons or protons only). An insight to this issue is given at the end of this Section.

The vanishing values of the thermal conductivity across a well established *lasagna* (say, for $T < 1\,\mathrm{MeV}$) can be easily explained because of the existence

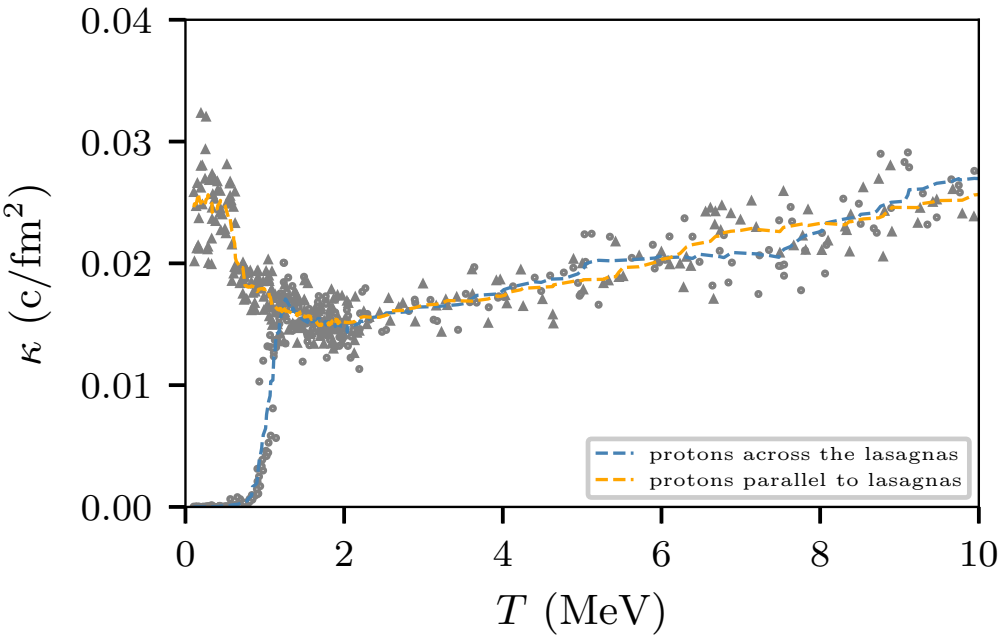

(a) wide view

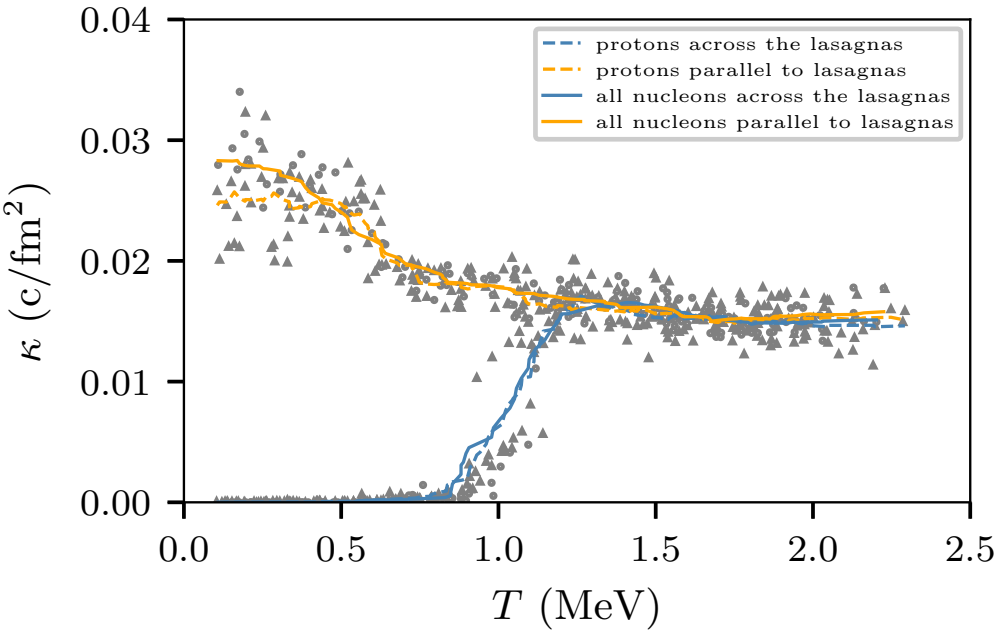

(b) detailed view

Figure 2: (On-line color only) Thermal conductivity κ vs. temperature during the heating evolution after the *lasagna* was established. The system density was $\rho = 0.05$ ($x = 0.5$). The smoothening was done following a moving average procedure of ± 10 points. The rounded gray points correspond to the raw data obtained over *all* the nucleons. The triangular gray points correspond to the raw data obtained over *protons* only.

of voids between the slabs (see Fig. 3). The negative slope for the parallel κ (*i.e.* along the *lasagna*) means that the "solid pasta" presents an enhanced conductivity with respect to the "liquid pasta". This behavior is common to other materials.

The slab structure of the *lasagnas* undergoes openings for decreasing densities in the simulation cell. Fig. 3 shows how these openings spread over the slabs until the *lasagna* is no longer sustainable, moving to the *spaghetti*-like structure (see Fig. 3a). Fig. 4 exhibits the corresponding proton thermal conductivity (after the data smoothening).

The "decoupling" pattern goes through the explored densities (see Fig. 4), including either *spaghettis* or *lasagnas*. The "decoupling threshold" (say, $T \simeq 1.25\,\mathrm{MeV}$) remains unchanged (within the current measurement errors). The (parallel) thermal conductivity, however, exhibits a density dependency on either side of this threshold. According to Fig. 4, the parallel κ (protons only) increases for increasing densities all along the explored temperatures. The orthogonal κ (protons only) meet this behavior above the "decoupling threshold", that is, after the pasta breakdown occurs.

Notice that the solid-like state also attains some kind of density dependence for κ (protons only). The current fluctuations of our measurements does not allow to distinguish clearly between the corresponding thermal conductivity values at $\rho = 0.03$ (*spaghettis*) and $\rho = 0.04$ (washed out *lasagna*). But Fig. 4 shows fairly different values between $\rho = 0.03$ and $\rho = 0.05$.

We may summarize our results as follows. The *pasta* breakdown process (during a heating evolution) accomplishes a dramatic change in the thermal conductivity of symmetric neutron star matter. For "cold" *pastas*, the thermal conductivity is only possible along the *pasta* structure, attaining a "decoupling" between orthogonal directions. The solid state of "cold" *pastas* even enhances the conductivity. But warming the *pastas* above the threshold $T \simeq 1.25\,\mathrm{MeV}$, breaks down its topological structure, connecting regions that were once separated by voids. This situation allows heating on any direction, and thus, the thermal conductivity switches to an homogeneous (isotropic) value, that may depend on the system density.

4.2 The thermal conductivity κ of non-symmetric matter

The next step in the investigation focused on the thermal conductivity behavior for proton ratios varying from $x = 0.5$ down to $x = 0.3$. The nucleons' potentials remained unchanged, as expressed in Section 1. Fig. 5 shows the corresponding profiles (up-to the cut-off distance) in comparison with a *lasagna*-like background. Notice that the slabs widths do no exceed the cut-off distance, although they look more irregular than in the case of symmetric matter.

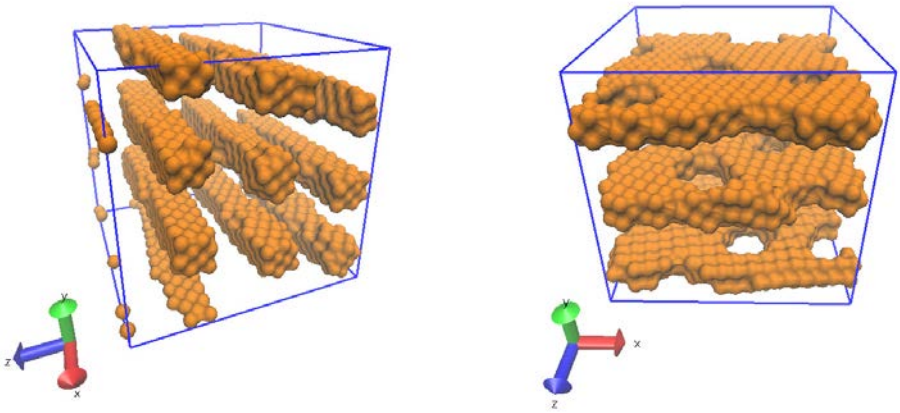

(a) $\rho = 0.03$ (b) $\rho = 0.04$

(c) $\rho = 0.045$ (d) $\rho = 0.05$

Figure 3: Surface plots for protons at $T = 0.1\,\mathrm{MeV}$ ($x = 0.5$). The nucleon densities are indicated below each snapshot.

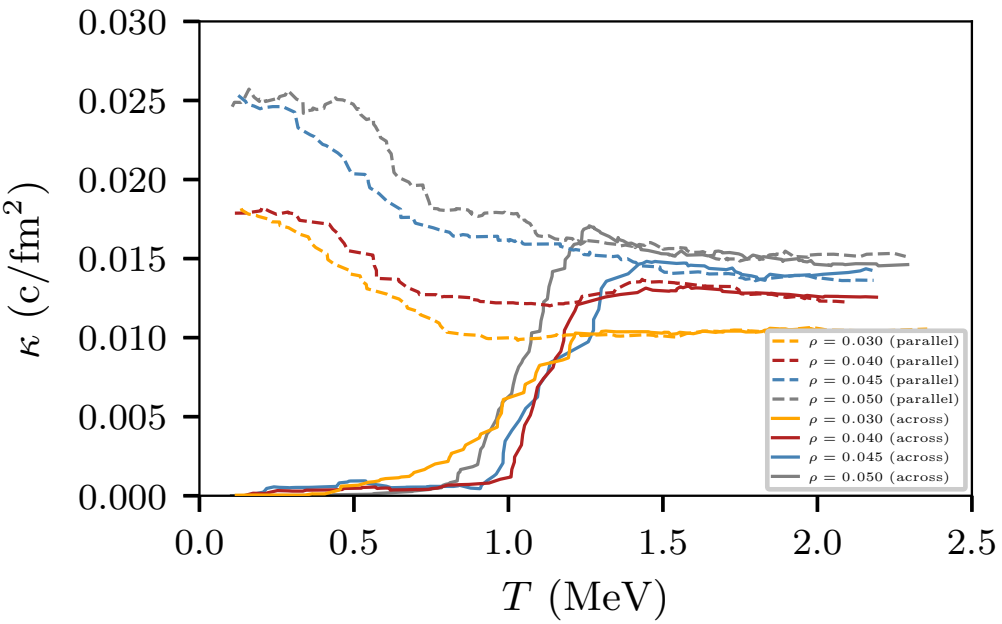

Figure 4: (On-line color only) Proton thermal conductivity κ vs. temperature for densities in the range 0.03 to 0.05 fm^{-3} and $x = 0.5$ (see insert for details). The smoothening was done following a moving average procedure of ± 10 points. The dashed lines correspond to the thermal conductivity values along (parallel) the pasta structure. The continuous lines correspond to the thermal conductivity across the pasta structure.

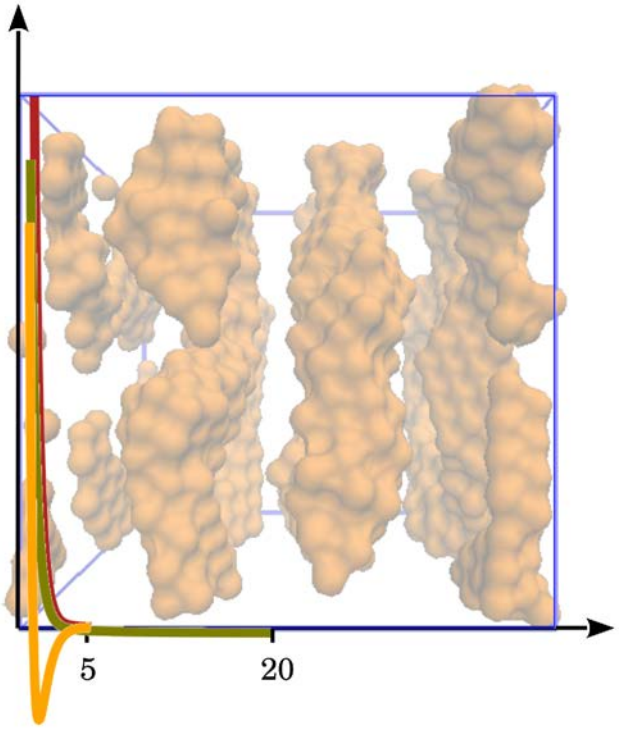

Figure 5: (On-line color only) Potentials as a function of distance (fm). The red curve corresponds to $V_{nn}(r)$, the orange curve corresponds to $V_{np}(r)$ and the green one to $V_{pp}(r)$ (includes the Coulomb contribution. The semi-transparent image in the background represents a *lasagna*-like structure for $\rho = 0.05$ and $x = 0.3$ (only protons are represented).

The thermal conductivity for non-symmetric neutron star matter was computed in the same way as in Section 4.1. Fig. 6 shows the proton thermal conductivity behavior for the $x = 0.3$ situation, evolving from "cold" (solid) temperatures to "warm" ones. The corresponding snapshots (protons only) are also exhibited.

Notice that the (qualitative) patterns appearing in Fig. 6 resemble those exhibited in Fig. 2 for the symmetric situation (and for similar density). The proton conductivity across the slabs vanishes. Besides, the conductivity "decoupling" is present on either symmetric and non-symmetric matter, in correspondence with the topological transformations. The "decoupling threshold" at this instance, however, appears somewhat biased with respect to the symmetric situation.

Fig. 7 brings out the complete picture for the proton thermal conductivity κ. Although the profiles are qualitatively similar, the asymmetric proton conductivity values scale down with respect to the symmetric proton conductivity. Say, the parallel conductivity for $x = 0.3$ (see Fig. 7) never surpasses

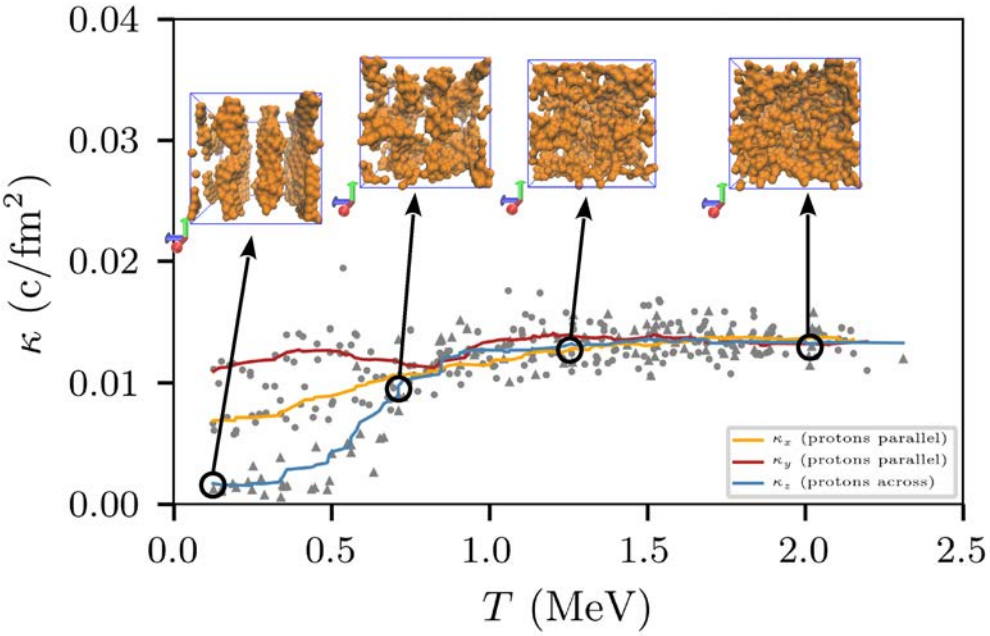

Figure 6: (On-line color only) Proton thermal conductivity κ vs. temperature for $\rho = 0.05$ and proton ratio $x = 0.3$. The smoothening was done following a moving average procedure of ± 10 points. The rounded gray points correspond to data obtained along the lasagna direction. The triangular gray points correspond to data across the lasagna structure.

$0.01\,\mathrm{c/fm^2}$, while the corresponding values for $x = 0.5$ appear always above. Furthermore, the later reports a maximum at the solid state ("cold" temperatures), while the former does not.

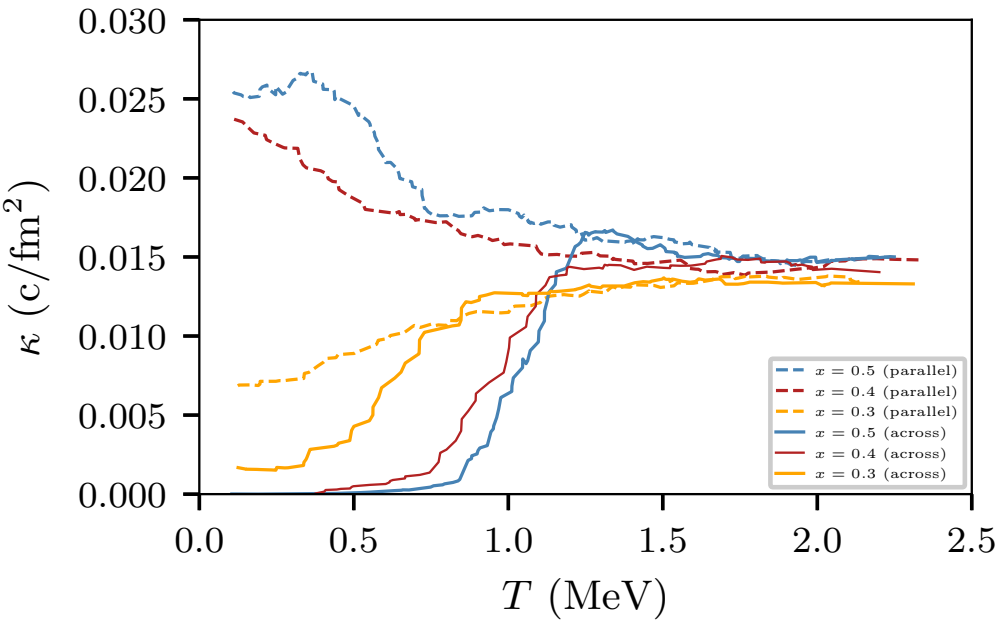

Figure 7: (On-line color only) Proton thermal conductivity κ vs. temperature for $\rho = 0.05$ and proton ratios in the range $x = 0.3$ to 0.5 (see insert for details). The smoothening was done following a moving average procedure of ± 10 points. The dashed lines correspond to the thermal conductivity values along (parallel) the pasta structure. The continuous lines correspond to the thermal conductivity across the pasta structure.

The overall thermal conductivity (that is, considering *all* the nucleons) appears to be very similar for symmetric and non-symmetric matter, at "warm" temperatures. The corresponding profile for $x = 0.3$ is shown in Fig. 8. The neutron thermal conductivity is also included. Both profiles are remarkably similar, meaning that the thermal conduction for $x = 0.3$ is mostly achieved by neutrons.

The above observations indicate that the thermal conductivity for non-symmetric matter shares the same qualitative behavior as the symmetric matter, despite that *pastas* are now embedded in a cloud of neutrons. The neutron thermal conductivity, though, resembles better the overall conductivity than the proton conductivity.

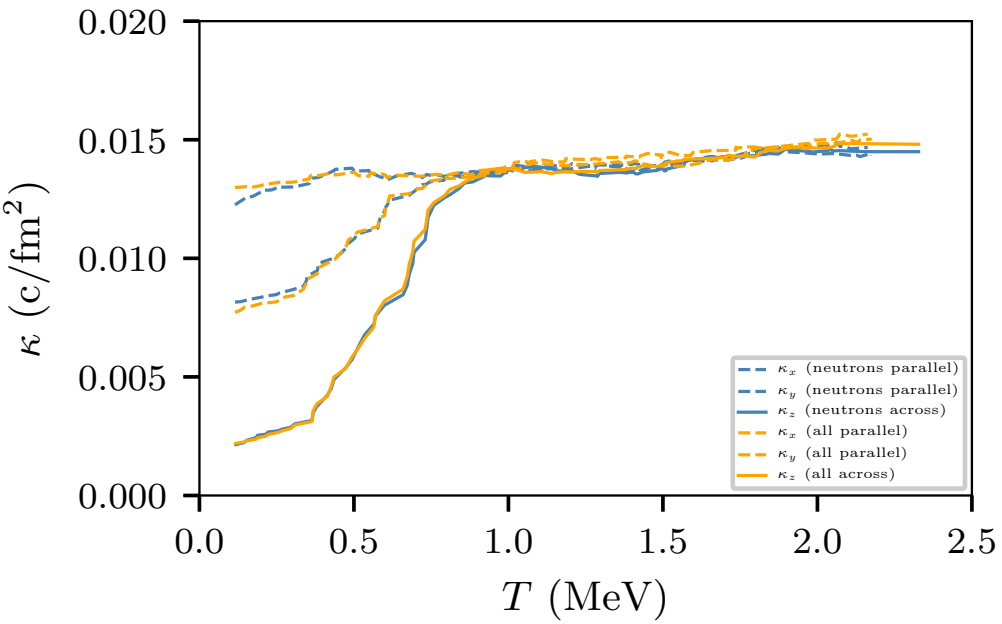

Figure 8: (On-line color only) Thermal conductivity κ vs. temperature for $\rho = 0.05$ and proton ratio $x = 0.3$. The blue lines correspond to the neutron conductivity, while the orange lines consider *all* the nucleons (see insert for details). The dashed lines (regardless for the color) correspond to the conductivity along (parallel) the spaghetti structure. The continuous lines, instead, correspond to any direction across the spaghetti structure. The smoothening was done following a moving average procedure of ± 10 points.

5. Conclusions

The thermal conductivity of *pastas* raises as a complex magnitude that is far from attaining a well established behavior. Researchers admit that variations of κ of (at least) an order of magnitude can be expected at sub-saturation densities, and temperatures below 2 MeV. The proton fraction is also a significant source of variations and a challenging field of investigation.

Since the *pasta* structures may become too complex for an increasing number of nucleons, we focused on simple structures (say, *lasagnas* and *spaghettis*) housing 4000 nucleons. We arrived to the main conclusion that the *pasta* breakdown process accomplishes a dramatic change of the phononic thermal conductivity. Neutron star matter switches from a strong non-isotropic regime (at the well-formed *pastas* regime) to an isotropic one, as temperature increases. This occurs sharply around $T \simeq 1\,\mathrm{MeV}$ for symmetric matter, and somewhat below this threshold for non-symmetric matter.

The above conclusion is a compelling reason for associating the *pasta* topological transition to low (or high) phononic thermal conductivities, although an estimate of the "effective" κ across the neutron star crust is not yet available. The *pasta* breakdown threshold, though, appears as a key issue for this estimate.

References

[1] C. J. Horowitz and D. K. Berry. Shear viscosity and thermal conductivity of nuclear pasta. Phys. Rev. C, 78:035806, Sep 2008.

[2] A. S. Schneider, D. K. Berry, M. E. Caplan, C. J. Horowitz, and Z. Lin. Effect of topological defects on nuclear pasta observables. Phys. Rev. C, 93:065806, Jun 2016.

[3] E Flowers and N Itoh. Transport properties of dense matter. ii. Astrophysical Journal - ASTROPHYS J, 230:847–858, 06 1979.

[4] P. B. Jones. Heterogeneity of solid neutron-star matter: transport coefficients and neutrino emissivity. Monthly Notices of the Royal Astronomical Society, 351(3):956–966, 2004.

[5] P. S. Shternin and D. G. Yakovlev. Electron-muon heat conduction in neutron star cores via the exchange of transverse plasmons. Phys. Rev. D, 75:103004, May 2007.

[6] P. S. Shternin, M. Baldo, and P. Haensel. Transport coefficients of nuclear matter in neutron star cores. Phys. Rev. C, 88:065803, Dec 2013.

[7] Alex Deibel, Andrew Cumming, Edward F. Brown, and Sanjay Reddy. Late-time cooling of neutron star transients and the physics of the inner crust. The Astrophysical Journal, 839(2):95, apr 2017.

[8] C. J. Horowitz, D. K. Berry, C. M. Briggs, M. E. Caplan, A. Cumming, and A. S. Schneider. Disordered nuclear pasta, magnetic field decay, and crust cooling in neutron stars. Phys. Rev. Lett., 114:031102, Jan 2015.

[9] C. O. Dorso, P. A. Giménez Molinelli, and J. A. López. Topological characterization of neutron star crusts. Phys. Rev. C, 86:055805, Nov 2012.

[10] C.O. Dorso, G.A. Frank, and J.A. Lpez. Symmetry energy in neutron star matter. Nuclear Physics A, 2019.

[11] C.O. Dorso, G.A. Frank, and J.A. Lpez. Phase transitions and symmetry energy in nuclear pasta. Nuclear Physics A, 978:35 – 64, 2018.

[12] Rana Nandi and Stefan Schramm. Transport properties of the nuclear pasta phase with quantum molecular dynamics. The Astrophysical Journal, 852(2):135, jan 2018.

[13] Hyoungchul Kim, Moo Hwan Kim, and Massoud Kaviany. Lattice thermal conductivity of uo2 using ab-initio and classical molecular dynamics. Journal of Applied Physics, 115(12):123510, 2014.

[14] Pradeep Kumar and H. Eugene Stanley. Thermal conductivity minimum: A new water anomaly. The Journal of Physical Chemistry B, 115(48):14269–14273, 2011.

[15] Jonathan M. Dunn. Nanoscale phonon thermal conductivity via molecular dynamics. Open Access Theses - Purdue e-Pubs, 766, 2016.

[16] Carlos Bertulani. Neutron star crust. Nova Science Publishers, Hauppauge, N.Y, 2011.

[17] P. N. Alcain, P. A. Giménez Molinelli, and C. O. Dorso. Beyond nuclear "pasta" : Phase transitions and neutrino opacity of new "pasta" phases. Phys. Rev. C, 90:065803, Dec 2014.

[18] J. A. López, E. Ramírez-Homs, R. González, and R. Ravelo. Isospin-asymmetric nuclear matter. Phys. Rev. C, 89:024611, Feb 2014.

[19] P. N. Alcain, P. A. Giménez Molinelli, J. I. Nichols, and C. O. Dorso. Effect of coulomb screening length on nuclear "pasta" simulations. Phys. Rev. C, 89:055801, May 2014.

[20] Florian Muller-Plathe. A simple nonequilibrium molecular dynamics method for calculating the thermal conductivity. J. Chem. Phys, 106(14):6082 – 6085, 1997.

[21] Ya Zhou, Benjamin Anglin, and Alejandro Strachan. Phonon thermal conductivity in nanolaminated composite metals via molecular dynamics. The Journal of chemical physics, 127(18):184702, 2007.

[22] Jonathan Dunn, Edwin Antillon, Jesse Maassen, Mark Lundstrom, and Alejandro Strachan. Role of energy distribution in contacts on thermal transport in si: A molecular dynamics study. Journal of Applied Physics, 120(22):225112, 2016.

[23] Keng-Hua Lin and Alejandro Strachan. Thermal transport in sige superlattice thin films and nanowires: Effects of specimen and periodic lengths. Physical Review B, 87(11):115302, 2013.